Journal of Electronic Materials (2024) 53:6269–6281
https://doi.org/10.1007/s11664-024-11317-0

ORIGINAL RESEARCH ARTICLE

Defect Engineering in Diamond-Based Semiconductors: Exploring the Role of Lithium Vacancy Defects

Tahani Saad Almutairi[1]

Received: 19 December 2023 / Accepted: 5 July 2024 / Published online: 21 July 2024

Abstract

Understanding the properties of lithium vacancy, Li_CV, defects in diamond is crucial for optimizing diamond-based semiconductor performance and unlocking its full potential in advanced electronic applications. In this study, we present a comprehensive theoretical investigation of the neutral Li_CV defect, resulting from the interaction between a lithium substitutional and a vacancy, in diamond. Employing periodic supercell calculations, we utilize global (B3LYP and PBE0) and range-separated (HSE06) hybrid functionals, as well as a local basis set, within the $CRYSTAL_{17}$ code to analyze the relaxed lattice structure, formation energy, magnetic properties, and electronic structures of Li_CV and other related isolated defects (Li_C V and 2V). Our results reveal that Li_CV exhibits three distinct spin states (doublet, quartet, and sextet) with significant differences in spin density distributions on first-neighbor carbon atoms. The quartet state is energetically favored by 0.09 eV and 0.88 eV (B3LYP) compared to the doublet and sextet states, respectively. The Li atom is positioned midway between the two vacancies in the Li_CV defect, exhibiting a local D_{3d} symmetry. Our findings reveal that the Li_CV defect exhibits remarkable stability within the diamond matrix, with its dissociation into Li_C and a vacancy (V) demanding a substantial energy barrier of 6.07 eV. In environments rich in vacancies, Li_C shows a strong preference for binding with these vacancies, thereby facilitating the formation of Li_CV complexes. Raman scattering calculations offer intriguing insights into the Li_CV defect, revealing distinctive spectral features that significantly aid in distinguishing this particular defect among isolated lithium Li_C and vacancy (V) defects. This observation is crucial, especially considering the challenges in fabricating shallow donors involving interstitial lithium in diamond, where preexisting vacancies can significantly influence the process. The comprehensive analysis provided in this study not only deepens our understanding of the Li_CV defect and its physical properties but also enhances our ability to detect this defect during the synthetic process, and to precisely control the formation conditions. This capability is vital for optimizing the electronic properties of diamond for advanced technological applications.

Keywords Vacancy · defect · formation energy · binding energy · band structure

Introduction

Defects are of paramount importance in numerous industrial applications across physics and chemistry, including electronics and photocatalysis. They enable the tailoring of advantageous properties such as doping, creating color centers for quantum applications, and enhancing semiconductor conductivity. Diamond electronic materials have emerged as promising candidates for advanced applications, owing to their exceptional properties, such as high thermal conductivity, high breakdown voltage, and wide bandgap.[1–5] However, to fully exploit these materials, dopants must be incorporated into the correct crystal sites.

Phosphorus has been reported as the sole donor providing *n*-type conductivity in diamond,[6–11] but it presents challenges, including a deep donor level and induced crystal strain.[12–18] In contrast, *p*-type conduction is readily achieved in diamond with boron doping.[19–24] Researchers have explored alternative dopants, such as Li, to attain *n*-type conductivity in diamond. Li has been considered as a single dopant in tetrahedral interstitial sites (Li_I)[25,26] or in complexes with nitrogen atoms (LiN_4).[27] The calculated donor level of Li_I was found to be between 0.1 eV and 0.6 eV[25,28–31] and 0.2 eV for LiN_4[27], below the conduction

✉ Tahani Saad Almutairi
talmutairi@taibahu.edu.sa

[1] Chemistry School, Taibah University, Madinah, Saudi Arabia

band, making this defect a promising candidate for *n*-type conductivity.

Lithium incorporation into diamond crystals can occur during CVD growth, implantation, or diffusion. Ion diffusion is commonly preferred for doping semiconductors, as it causes less damage than ion implantation.[32–38] The diffusion of Li into high-quality natural diamond crystals has been achieved using various solid materials.[36,37,37,39–41] In theory, Li can readily diffuse through the crystal between two tetrahedral interstitial sites with calculated activation energy, 1.1,[29] 0.85,[25,28] 1.09[29] , and 1.3 eV.[31,42] Experimental values for Li diffusion are close to these theoretical values, 0.9 ± 0.3 eV[40] and 0.26 eV[37]. Studies suggest that crystal defects contribute to Li atom binding and reduced diffusion, particularly at higher temperatures where defect mobility increases.[34]

Despite extensive simulations conducted on individual lithium interstitial (Li_I) and lithium substitution (Li_C) defects in diamond, as documented in various studies,[27,29,31,43,44] the interaction between Li_C and vacancies (V) to form lithium vacancy (Li_CV) defects remains largely unexplored. The formation of Li_CV defects during synthesis or annealing processes can restrict the generation of lithium interstitials. This limitation reduces the availability of shallow donor states, which are predicted to be located at 0.1 eV,[25,28] 0.35 eV[29] , and 0.4 eV[30] below the conduction band. Consequently, this can potentially curtail the performance enhancements that these donor states could otherwise facilitate. Therefore, acquiring a comprehensive understanding of Li_CV defects and their formation mechanisms is critical, not only for optimizing the electrical properties of diamond but also for enhancing its application in semiconductor technologies. This study aims to provide crucial insights into the development of high-performance diamond-based devices. We perform theoretical calculations to determine the geometry, energy, stability, and electronic, magnetic and vibrational properties of Li_C, a neutral vacancy (V), two nearest neighbor vacancies (2 V), and lithium vacancy (Li_CV) defects in diamond, utilizing various hybrid functional methods. By examining the formation, distribution, and properties of Li_CV defects, we can develop strategies to mitigate their effects and unlock the full potential of diamond for semiconductor applications. This research will also contribute to the broader field of defect engineering, paving the way for the design of more efficient, durable, and environmentally friendly electronic devices that can withstand harsh conditions and meet the demands of emerging technology sectors.

Computational Details

The density functional theory (DFT)[45,46] presented in this study relies on the widely recognized global hybrid functional, B3LYP,[47] as implemented in the $CRYSTAL_{17}$ code.[48] To compare defect energy results, other DFT formalisms such as PBE0[49] and range-separated HSE06[50] were incorporated, providing a more accurate understanding of electronic spin localization. The selection of B3LYP, PBE0, and HSE06 was driven by their distinct approaches to incorporating exchange–correlation effects, which are crucial for accurately describing the electronic properties of defects in semiconductors. Each method offers unique strengths in handling the complex interactions within the Li_CV defect, thereby providing a comprehensive understanding through complementary perspectives. By employing these three methods, our study leverages the strengths of each to validate and cross-verify the electronic properties and stability of the Li_CV defect. The complementary insights gained from these methods enhance the reliability of our predictions and provide a more nuanced understanding of the defect's behavior in diamond. The basis sets chosen in this study for Bloch function expansions were for C, 6-21G,[51,52] and for obtaining a detailed representation of the interaction between Li and C atoms, triple-zeta valence with polarization (pob_TZVP).[53] The vacancies were modeled by removing the designated atoms, which involved eliminating the nuclei, electrons, and basis set. All defects examined in this study were spin-polarized open-shell systems, to which we applied spin-unrestricted hybrid functionals. Full optimizations, comprising lattice parameters and all atomic bases, were conducted using a root mean square displacement of 10^{-5} Å. The computational parameters employed in this study encompassed five values (T1–T5), which were set as 10^{-7} (T1–T4) and 10^{-14} (T5)[48]. These criteria govern the truncation of the (infinite) Coulomb and exchange series. The self-consistent field (SCF) threshold energy was set to 10^{-8} and 10^{-10} Hartree in optimization and vibration frequency calculations, respectively. The default is 10^{-6} Hartree. The number of independent k-points has been determined by the shrinking factors utilized in the sampling of the Monkhorst–Pack grid[54,55] and is set to 44, which corresponds to 36 points in the first Brillouin zone with the Li_CV defect when no symmetry constraints are applied. Mulliken population analysis for charge and spin density was executed at the end of the SCF process for each non-equivalent atom.[48,56] The spin densities were specified solely for the atoms in the defect region (e.g., first-neighbor carbon atoms) in the initial guess, α (+1) and spin β (−1), to define the open-shell configurations. The calculated lattice parameters (Å) of the undefective diamond were (3.59, B3LYP), (3.57, HSE06), and (3.57, PBE0), which were within 0.6–0.08% of the experimental value, 3.567.[57] The obtained bandgaps (in eV) for the undefective diamond cell were (5.71, B3LYP), (5.15, HSE06), and (5.79, PBE0), which align well with previously reported values using the same levels of theory, (5.73, B3LYP), (5.17, HSE06), and (5.80, PBE0)[58] (the

measured value 5.4–5.6 eV[59,60]). The formation energy of the defects was computed using:

$$\Delta E_f = E_{tot}^{Def} - E_{tot}^{UND} - \sum n_I \mu_I \quad (1)$$

where E_{tot}^{Def} and E_{tot}^{UND} are the total energies of defective and undefective diamond supercells, respectively, and μ_I is the chemical potential of the n_I atom (added or removed from the cell), which was taken as the energy per atom of the bulk diamond for C and the energy per atom in the most stable solid form of Li (BCC) for the Li atom. The stability of the defect *AB* is commonly examined by calculating the dissociation energy (binding energy) of the defect using:

$$E_d^{AB} = (E_{tot}^{A} + E_{tot}^{B}) - E_{tot}^{AB} \quad (2)$$

where E_{tot}^{AB}, E_{tot}^{A} and E_{tot}^{B} are the total energies of defect *AB* and its isolated *A* and *B* forms in diamonds, respectively.

The wavenumbers, denoted as ωp, were derived from the second derivatives of energy with respect to atomic displacements, u, at the Γ point, as referenced in sources.[61,62] These calculations are captured in:

$$W_{ai,bj}^{\Gamma} = \frac{H_{ai,bj}^{0}}{\sqrt{M_a M_b}} \quad \text{where } H_{ai,bj}^{0} = \frac{\partial^2 E}{\partial u_{ai}^{0} \partial u_{bi}^{0}} \quad (3)$$

In the context of these equations, u represents the displacements of atoms a and b within the system, each associated with their respective atomic masses. The subscripts I and j are indices representing the coordinates of these atoms. This analysis employed a coupled Perturbed–Hartree–Fock/Kohn–Sham approach, cited in references,[63,64] to not only calculate the integrated intensity for infrared absorption but also to analytically evaluate the Raman intensities.

Results and Discussion

Substitutional Lithium, Li_C and Vacancy defect, V

This section reports the results related to the final optimized structure obtained from B3LYP calculations (64 supercells). The incorporation of Li into the substitutional site generates five electrons, leading to two stable spin states: quartet ($S_Z = 3/2$) and doublet ($S_Z = ½$), with the former being 0.05 eV lower in energy (Table I), consisting of the previous calculation on the same defect.[65,66]

Figure 1 provides further details on the charge and spin distributions, bond lengths, and angles of the first and second carbon shells. The Li-induced lattice perturbations diminish quickly, with bond lengths in the second and third shells returning to approximately 1.51 Å and 1.56 Å, respectively. Such short-range perturbations are typically observed with smaller substitutional atoms, such as boron (B) and nitrogen (N),[67–72] which induce minimal distortion within the host lattice. The limited spatial extent of these perturbations suggests that the Li atom integrates smoothly into the lattice, maintaining much of the original structural integrity. This behavior is significant, as it indicates that the electronic and structural properties of the material can be modified without introducing extensive disruption. Consequently, this can be advantageous for applications requiring precise modifications of material properties, such as in semiconductor doping.

Table I Total energy and relative energies of Li-substituted defects in diamond: a comparison of different spin states

Functional	Supercell	The relative energy (eV) E ($S_Z = ½$) − E ($S_Z = 3/2$)
B3LYP	64	0.052 [0.07][65] [0.02][42] [0.015][44]
	128	0.057
HSE06	64	0.054
PBE0	64	0.041

The vacancy defects exhibit three distinct spin states: singlet, triplet, and quintet. The singlet state is energetically favorable, being lower by 1.4 eV and 0.1 eV compared to the quintet and triplet states, respectively. These values are in good agreement with those previously reported in the literature.[73–77] Each of the spin states induces outward relaxation of the lattice, with the quintet state causing the maximum distortion, while the singlet and triplet states lead to comparatively smaller relaxations. In terms of the charge distribution around the defect, the vacancy itself and its neighboring atoms exhibit a negligible charge, with less than 0.1|e| detected. This indicates that the defect does not significantly alter the charge state of its immediate environment. The spin density, as determined by Mulliken population analysis, shows strong localization at the four carbon atoms surrounding the defect. Specifically, in the quintet state, the spin density is 0.85|e| at each of the four carbon atoms. The triplet state has a spin density of 0.73|e| at three of the carbon atoms and − 0.40|e| at the remaining carbon atom. For the ground singlet state, the spin density is divided equally between two pairs of carbon atoms with opposite spins, with each pair having a spin density of 0.67|e| and − 0.67|e|.

Figure 2 presents a detailed comparison of the B3LYP band structures for the Li_C defect in various spin states and the corresponding V defect, revealing key differences in defect energy levels and electronic configurations. The observed shift in the energy of the Li electrons into the antibonding a_1 state, which moves its energy below the Fermi level, results in an altered electronic configuration ($a_1^2\, t_2^3$ instead of $a_1^1\, t_2^3$ in V[77]). This shift not only affects the basic electronic properties but also has significant implications for the material's optical and electronic device applications.

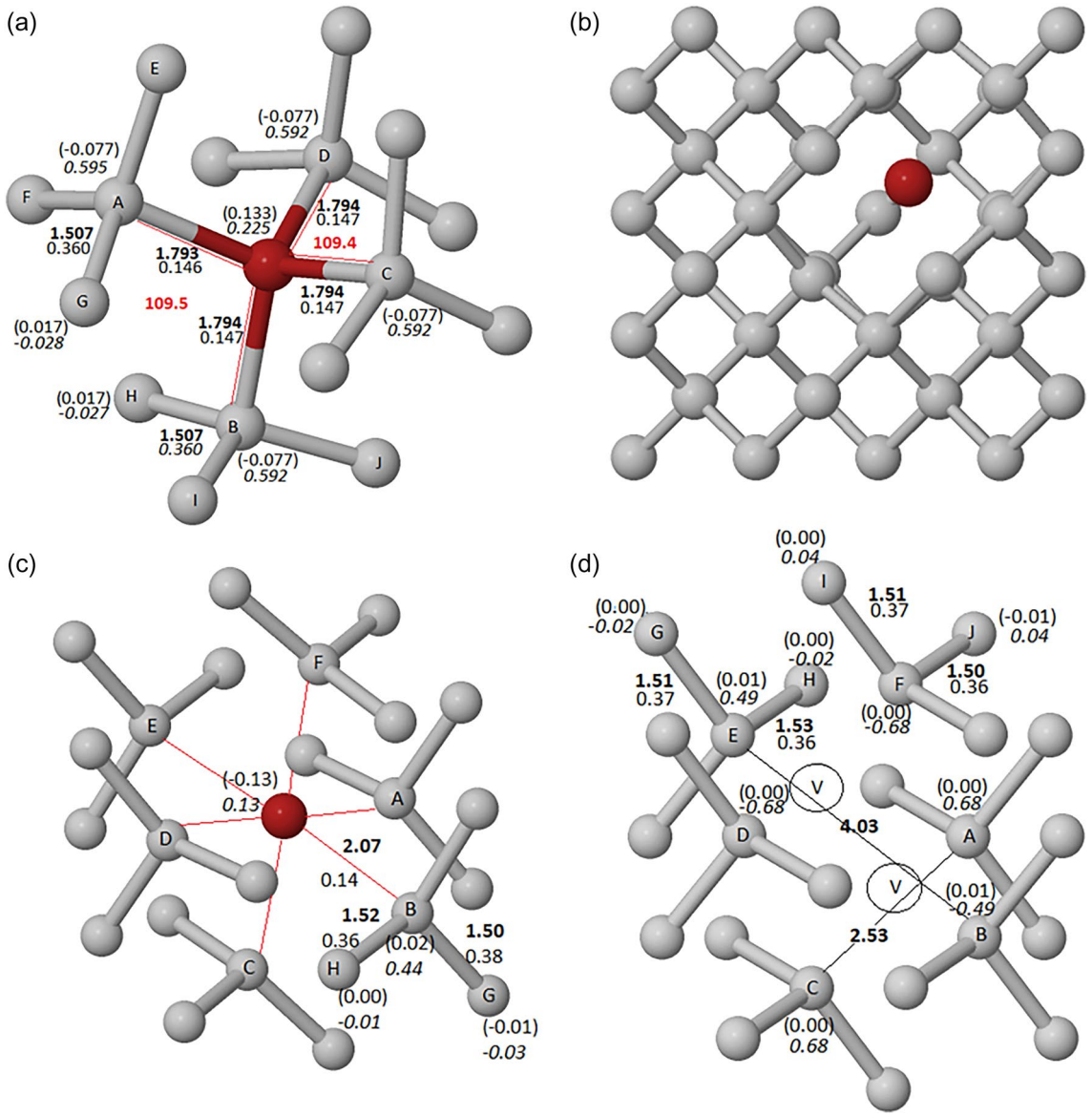

Fig. 1 Schematic of bond lengths (*in bold*), populations, angles (*red*), Mulliken charges (in parentheses), and spin momenta (in *italics*) for Li-related refects in damond:. (a) Li_C, (c) LiV, and (d) 2 V defects; (b) depiction of Li atom settling in the cavity of two vacancies. Data obtained using B3LYP and 64-atom supercells (Color figure online).

The antibonding t_2 shows lower energy and greater separation from the bottom of the conduction bands, approximately 2.8 eV, in the Li_C ($S_Z = 3/2$). The vertical optical excitation from the highest occupied level to the bottom of the conduction bands was 5.02 eV. In the Li_C ($S_Z = ½$), a structure similar to that of the corresponding V ($S_Z = 1$)[66,77] was found. The electronic structure of the V triplet persisted in C_{3V} symmetry. It displays one fully occupied a_1 level at the top of the valence bands, and a half-occupied doubly degenerate e_1 level below the Fermi level.[66] In the corresponding Li_C bands, the Li electron occupies the β spin of a_1 level that appears in the V gap, lowering its energy below the Fermi level.

These electronic comparisons underscore the technological relevance of tailoring the electronic properties of diamond through defect engineering, offering paths to novel applications in electronics, optoelectronics, and quantum information science. This study not only contributes to our fundamental understanding of defect dynamics in semiconductors but also highlights the practical implications of these defects in enhancing the functionality and application scope of diamond-based materials.

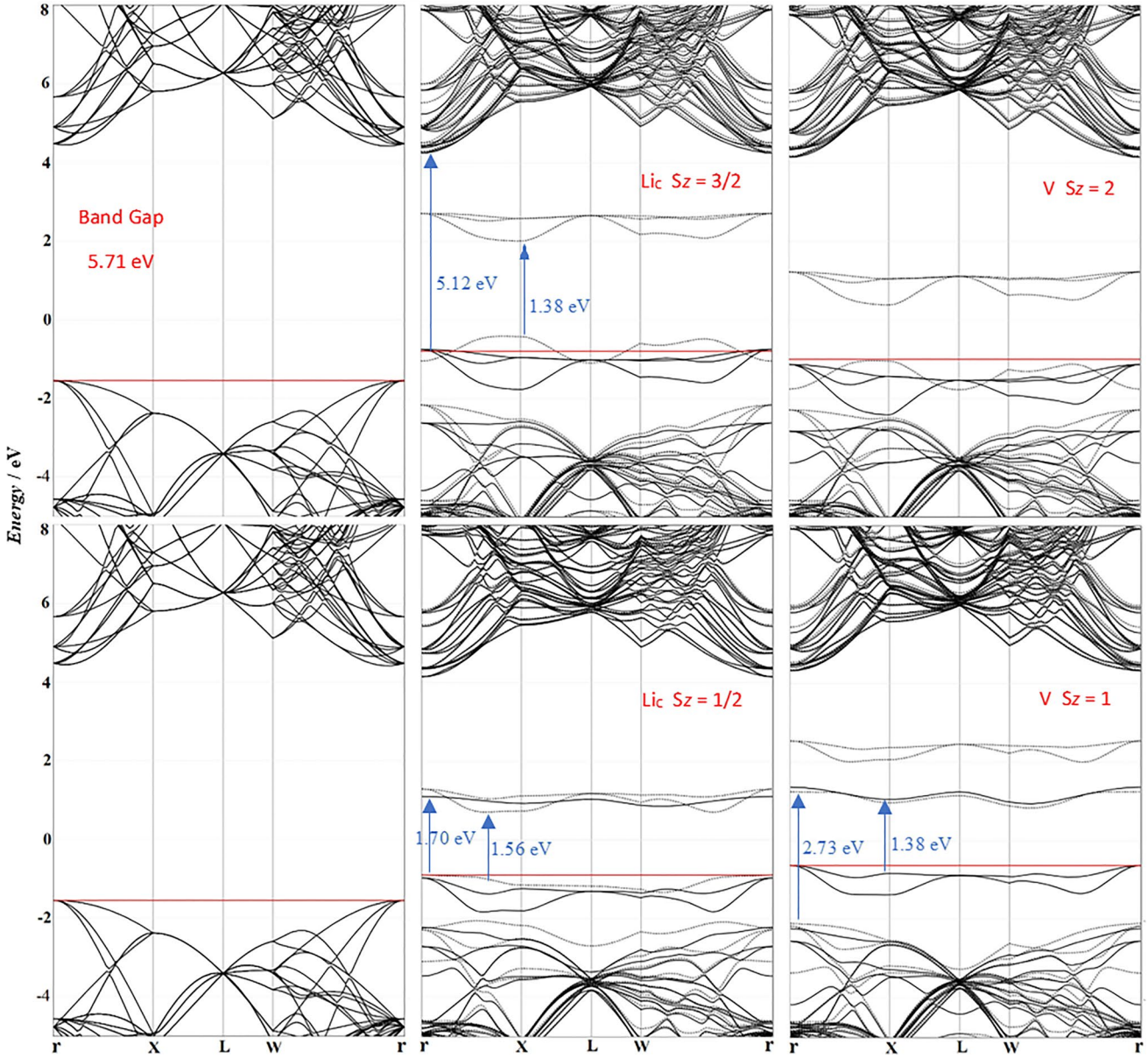

Fig. 2 Band structure comparison of undefective diamond, Li_C defects in various spin states, and corresponding isolated vacancy defects. Calculations performed using B3LYP functional and 64-atom supercells. *Horizontal red lines* represent the Fermi level; *continuous and dotted black lines* indicate α and β energy levels, respectively (Color figure online).

Lithium Vacancy Defect, Li_CV

The local geometries of the fully relaxed Li_CV structure are presented in Fig 1c. For comparison, the Li_CV defect can be analyzed alongside a 2 V defect, as shown in Fig. 1d. The 2 V defect generates six unsaturated bonds, with their six electrons capable of coupling to three possible spin states. The singlet ($S_Z = 0$) (3α, 3β) is found to be lower in energy by about 2.14 and 0.06 eV (B3LYP) than the septet ($S_Z = 3$) (6α) and triplet ($S_Z = 1$) (4α, 2β) states, respectively (Table II), consisting with previous reported values.[78]

Table II Total energy of 2V defect in diamond across various spin states and relative energy to singlet ground state

Functional	$E_{Triplet} - E_{Singlet}$ (eV)	$E_{Septet} - E_{Singlet}$ (eV)
B3LYP	0.059 [0.060][82]	2.141 [2.152][82]
HSE06	0.068	2.198
PBE0	0.059	2.125

In the singlet state, the spin arrangement is as follows: three carbon atoms on one vacancy side carry (2α, 1β) spins, while the other three carry opposite spins (2β, 1α). Mulliken analyses reveal high-spin localizations with densities of (+ 0.68|*e*|, − 0.49|*e*|, + 0.68|*e*|) and (− 0.68|*e*|, + 0.49|*e*|, − 0.68|*e*|). No significant charge change is observed at 2 V, as the net charge on the C atoms of the first and second neighbors is nearly zero (0–0.01|*e*|). The 2 V defect results in outward relaxation, with the C_E–C_B distance increasing from 3.92 Å in a perfect diamond to 4.03 Å, while the C_C–C_A distance remains constant at 2.53 Å. This relaxation leads to compression in the first shell bonds by approximately 1.68–3.59%, which is quickly restored in the second shell.

The Li_CV defect involves a lithium atom contributing one electron to terminate one of the unsaturated bonds at 2 V. This defect converges with three spin states: a doublet ($S_Z = ½$), quartet ($S_Z = 3/2$), and sextet ($S_Z = 5/2$). The relative stabilities of the three spin states obtained using these three functionals are listed in Table III. The quartet configuration is lower in energy by about 0.09 eV and 0.88 eV (B3LYP) than the doublet and sextet configurations, respectively. This observation highlights a state consisting of the magnetic properties of Li_CV and the basic Li_C, which also stabilize in a high-spin (quartet) state.[65,79] The magnetic behavior of Li_CV and Li_C is primarily due to how the electrons from the lithium and the vacancy interact within the diamond lattice. These interactions affect the spin states and magnetic properties of the material, making Li_CV potentially more complex and varied in magnetic behavior compared to the simpler Li_C configuration. The relatively small energy gap of 0.09 eV (equivalent to 1044 K) between the quartet and doublet states suggests the presence of strong spin–phonon coupling, a phenomenon typically observed in systems containing transition metals or rare-earth elements.[65,80]

Starting with the ground configuration, $S_Z = 3/2$, the Li atom occupies a midpoint in the cavity of the two vacancies, leading to six equal Li-C distances (2.07 Å) with D_{3d} symmetry. The net Mulliken charge exhibits an equal charge distribution on the first-neighbor carbon atoms: approximately 0.02|*e*| on each one and − 0.13|*e*| accumulated charge on the Li atom. The compression in the first shell bonds is minimal, approximately 2.3–3.5%, which nearly disappears in the second shell bonds. All six first-neighbor carbon atoms exhibit a highly localized α spin, 0.44|*e*|, and approximately 0.13|*e*| on the Li atom, which is nearly half the corresponding spin on Li_C.

Table III Total energy and relative energies of Li_CV defects in diamond: a comparison of different spin states with respect to the quartet ground state

Functional	SC	$E_{Doublet} - E_{Quartet}$ (eV)	$E_{Sextet} - E_{Quartet}$ (eV)
B3LYP	64	0.09	0.88
	128	0.08	0.89
HSE06	64	0.16	0.99
PBE0	64	0.04	0.79

The bond populations between the Li atom and the first-neighbor carbon atoms are less than the corresponding values in a perfect lattice (0.347|*e*|), approximately 0.14|*e*|, and display nearly the same value in the Li_C defect. The spin configurations in the Li doublet are found to be different: on each side of the Li atom, two of the first-neighbor C atoms carry α (0.490|e|) and one carries β (− 0.505|*e*|), ($\alpha\beta\alpha$), ($\alpha\beta\alpha$), with a small value on the Li atom (− 0.035). These distributions cause the two Li-C(β) distances to elongate by about 1% (2.09 Å) compared to the others that remain unchanged (2.07 Å), reducing the symmetry of the system. The charge on Li is − 0.12|*e*|, and those on αC and βC are − 0.001|*e*| and 0.04|e|, respectively. In the Li-sextet, the net spin per cell is 5|*e*|, distributed on the Li atom (0.29|*e*|) and the first-neighbor carbons (3C (α) 0.614|*e*| and 3C (α) 0.754|*e*|). All the Li–C distances show elongation, approximately 1.93% with C atoms carrying higher spin and approximately 1% with those carrying lower spin.

Figure 3 presents the band structures of Li_CV and 2 V defects in various spin states, calculated with B3LYP functional and 64-atom supercells. In the case of the 2 V singlet ($S_Z = 0$), configurations show six defective electrons pairing within three distinct bands located below the Fermi level. The uppermost of these bands approaches to just below the Fermi level, whereas the lowest band is visible at the Γ and L points, but absent at the X point. Above the Fermi level, three unoccupied bands are clearly delineated, showing a separation from the minimum of the conduction bands. The electronic configurations observed are consistent with previous computational study of the same system, affirming the reliability of the current results.[78] The resulting bandgap at the Γ point is notably smaller than that of the perfect crystal: 1.68 eV (B3LYP), 1.77 eV (PBE0), and 1.08 eV (HSE06) compared to 5.71 eV, 5.79 eV, and 5.15 eV, respectively.[58,81]

In the pristine condition, a single lithium (Li) atom in an interstitial site typically acts as a shallow donor within semiconductors, contributing to improved conductivity through extra electrons. However, our study demonstrates that, when this interstitial Li atom interacts with a vacancy (creating the Li_CV defect), the electronic properties are significantly altered. Incorporating a Li atom into the 2 V singlet's cavity adds an unpaired electron, leading to a possible doublet spin state ($S_Z = ½$) for Li_CV. In the Li_CV doublet, noticeable shifts occur between the α and β levels. Only two unoccupied bands appear above the Fermi level for the α spin, instead of three bands in the 2 V singlet. This results in four occupied bands below the Fermi level, with the top two bands being clearly distinguishable. The lower bands

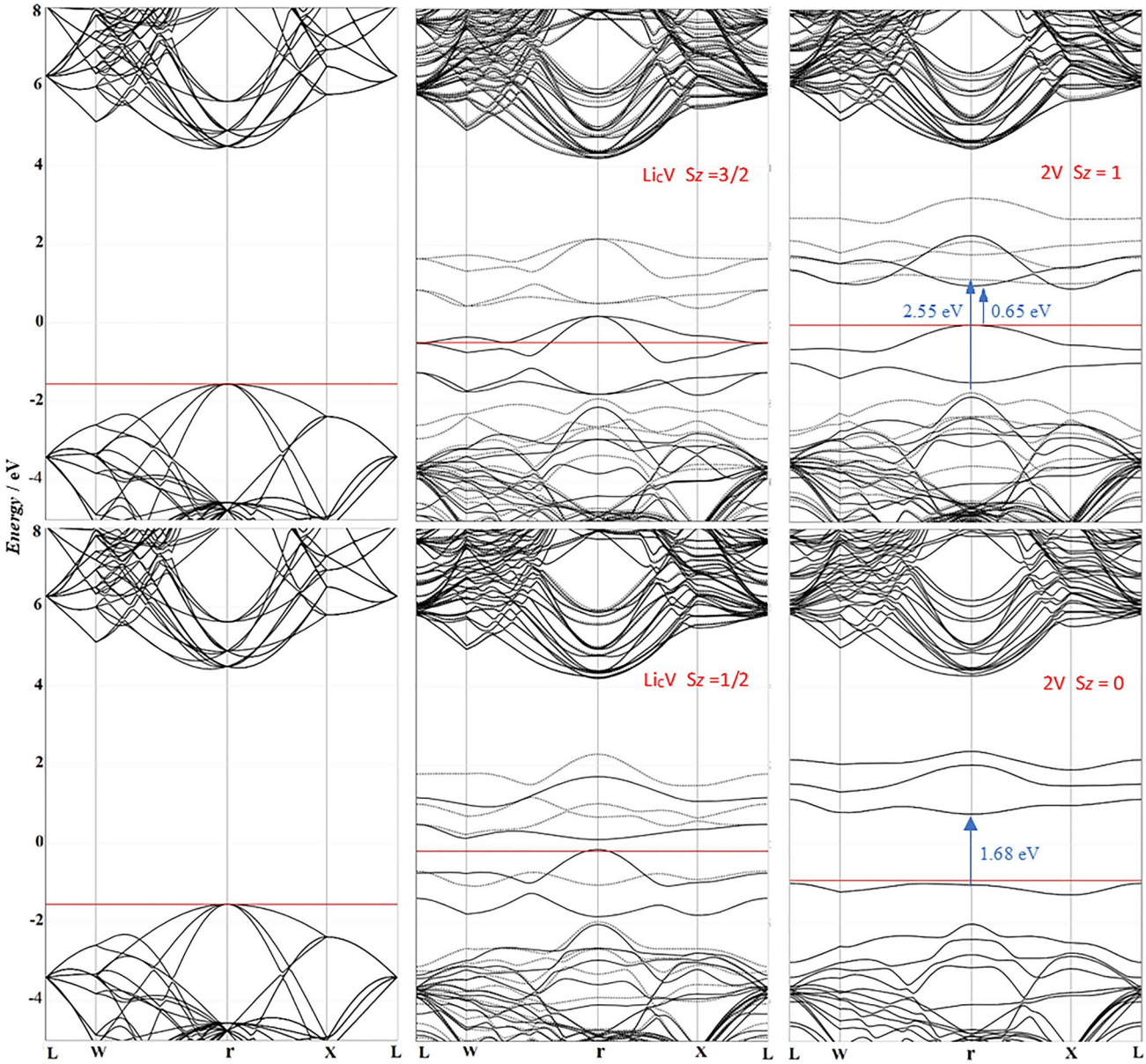

Figure 3 Band structure comparison of undefective diamond, Li_CV, and 2V defects. Calculations performed using B3LYP functional and 64-atom supercells. *Horizontal red lines* represent the Fermi level; *continuous and dotted black lines* indicate α and β energy levels, respectively (Color figure online).

merge with the top of the valence bands, as evident at the Γ point. The resulting gap for the α spin at Γ is very small: approximately 0.25 eV (B3LYP/64). Larger supercells (128-atom) yield small gaps of 0.27 eV and 0.60 eV for the α and β spin bands, respectively. With the HSE06 functional, the system becomes conductive due to the small bandgap of the perfect cell, and, with PBE0, the gaps are 0.23 eV and 0.49 eV, respectively. The reduction in the bandgap due to the Li_CV defect indicates a loss of the effective shallow donor behavior of the Li interstitial. The merging of the bands at the top of the valence band effectively reduces the ability of the semiconductor to transport charge efficiently, as the reduced bandgap leads to increased recombination rates of charge carriers. This makes the semiconductor less effective for applications requiring high conductivity and low recombination rates, such as in photovoltaic cells and other electronic devices.

For the 2 V triplet ($S_Z = 1$), two levels below the Fermi level are half-filled with two electrons, and the corresponding β spin bands appear in the antibonding range just above the Fermi level. The bandgaps in this system are reduced to 0.65 eV and 2.55 eV for the α and β bands (B3LYP),

respectively; 0.99 eV and 2.83 eV (PBE0) and 0.32 eV and 2.25 eV (HSE06). In Li_CV, ($S_Z = 3/2$), the gap has two doubly degenerate levels. The Li atom's electrons increase the half-filled levels in the 2 V triplet to three below the Fermi level, creating the most stable high-spin configuration, and their overlap results in a conductive system. The average energy levels obtained from the 128-atom band structure are presented in Fig. 4.

The interaction between Li and vacancies introduces states within the bandgap of the semiconductor. These states

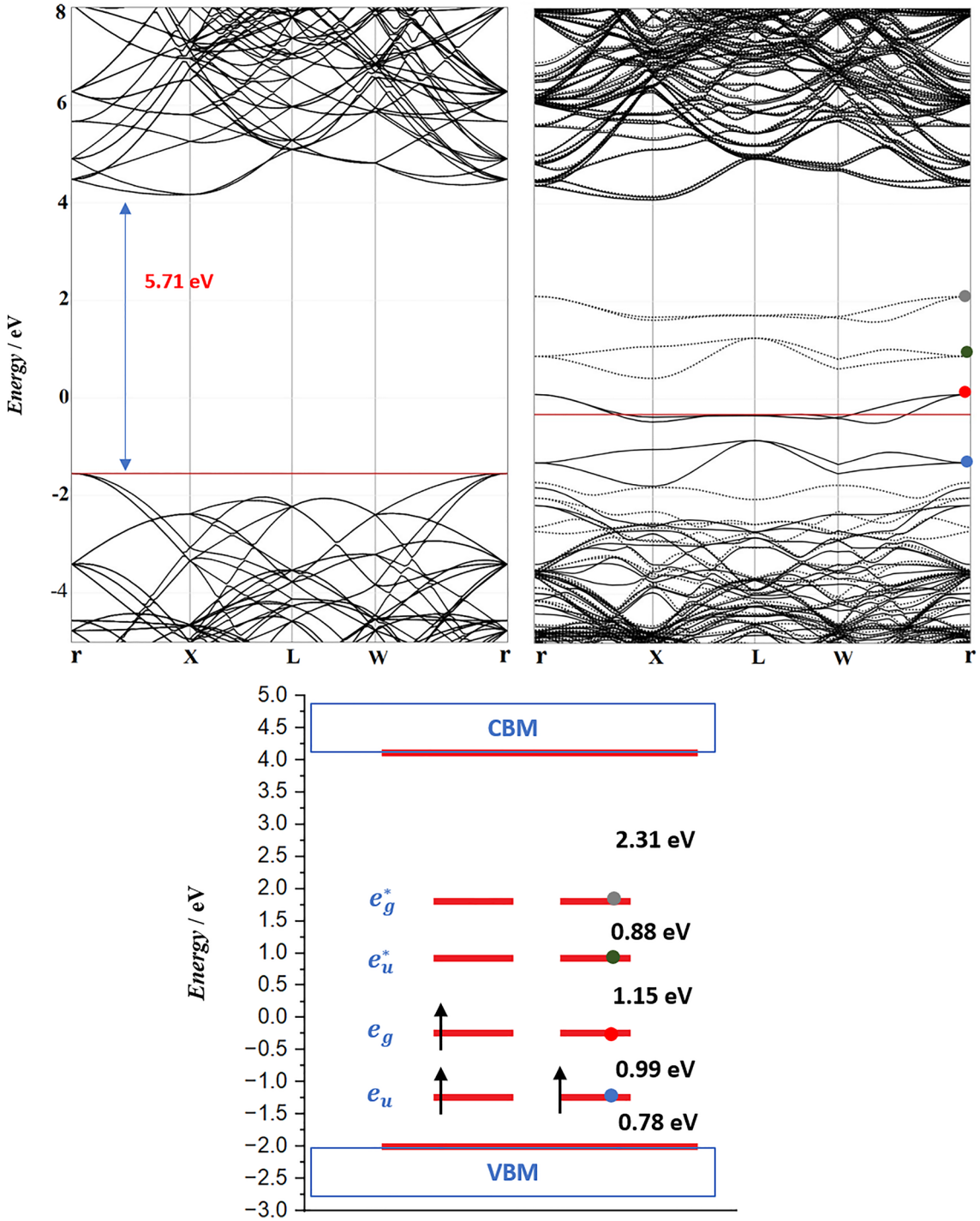

Figure 4 *Top panel* comparison of Li_CV (*right*) and undefective diamond (*left*) band structures obtained with 128-atom supercell and B3LYP. *Bottom panel* schematic of defect-related levels near the bandgap for Li_CV defect with *Sz* = 3/2. Valence band maximum (*VBM*) location taken at r point. *Colored circles* correspond to averaged levels with matching bands (Color figure online).

are typically localized around the defect site. These mid-gap states can act as traps for charge carriers (electrons and holes), which increases the probability of recombination. Unlike conduction or valence band states, carriers in these mid-gap states are spatially localized and have a higher likelihood of encountering a carrier of opposite charge, leading to recombination. In addition, the reduction in bandgap facilitates easier transition of electrons from the valence band to the conduction band. A smaller bandgap also means that thermal generation of carriers can occur more readily, increasing the population of free carriers available for recombination. Understanding these interactions and their implications allows for the strategic engineering of materials to mitigate adverse effects.

Formation and Binding Energies

The formation energies of isolated defects, such as Li_C, V, 2 V, and Li_CV, have been calculated and are presented in Table IV, alongside previously obtained values for comparison. One suggested method for forming Li_C in diamond involves trapping Li_I at a pre-existing vacancy,[42–44] where the Li in diamond is viewed as interstitial Li at the vacancy site. The binding energy between Li_I and V, required to form Li_C according to the reaction $Li_I + V = Li_C$, was found to be approximately 6 eV.

This value is nearly equal to the formation energy of vacancies, suggesting that defects Li_I and Li_C have very similar formation energies.[43] Calculations using the GGA functional yielded formation energy values of 8.4 eV for Li_I and 8.3 eV for Li_C.[44] In contrast, hybrid functionals detected a small difference between the Li_I and Li_C formation energies, with Li_I being approximately 0.5 eV (B3LYP) and 0.4 eV (HSE06) higher than Li_C.[44] In the present calculation, the formation energy of the Li_CV defect (9.20 eV, B3LYP) is found to be lower than that of the 2V defect (9.89 eV, B3LYP) by approximately 0.7 eV, both calculated within the same supercell size, indicating a small negative contribution from Li.

To evaluate the stability of 2 V and Li_C in diamond with respect to their dissociation into isolated defects (e.g., two V for a 2 V defect and Li_C and V for a Li_CV defect), binding energies were calculated for the following reactions: $V + V \rightarrow 2\ V$ and $Li_C + V \rightarrow Li_CV$ (Table IV). The obtained values reveal a high binding energy of 3.7 eV (B3LYP) for 2 V and a value of 6.07 eV (B3LYP) for Li_CV. This significant increase in binding energy from 3.7 eV to 6.07 eV suggests that it is more energetically favorable for mobile lithium atoms to occupy the cavity of 2 V. This occupation prevents further mobility and accounts for the substantial decrease in Li concentration beyond the diamond surface during the diffusion process.[36,37,40,41] Using the formation energy of Li_I from the B3LYP calculation[44] (9.1 eV), we estimated a binding energy of 9.79 eV between Li_I and 2 V for the reaction $Li_I + 2\ V \rightarrow Li_CV$. Pre-existing vacancies in bulk diamond likely play a crucial role in the interaction between diamond and lithium. This interaction can be enhanced by providing the system with the energy required to overcome the barrier for Li diffusion, which is quantified at approximately 0.9 eV $\pm$ 0.3 eV[40] and 0.26 eV.[37] These values are notably lower than those reported for a vacancy (V) defect, which stand at 2.3 eV $\pm$ 0.2 eV.[67] The addition of a Li atom into the dual vacancy (2 V) configuration, resulting in the formation of Li_CV, further stabilizes the system. This is demonstrated by the significantly higher binding energy of Li_CV, which is 6.07 eV, compared to 3.72 eV for the 2 V defect alone. This kind of dopant binding to vacancies and the subsequent aggregation phenomena are commonly observed with smaller dopants such as nitrogen (N).[83–85] However, this study is pioneering in illuminating the potential for similar aggregation processes with Li dopants and exploring their impact on the electronic and magnetic properties of diamond.

Spectroscopic Characterization: Probing Crystal Structures with Raman Spectroscopy

Raman spectroscopy provides a window into the intricate world of crystal structures, though assigning specific spectral features to distinct structural elements often presents experimental challenges. Factors such as preparation methods, temperature variations, defects, and inherent structural

Table IV Defect formation energy ($E_{f(x)}$) and binding energy (E_b) in diamond for various defect types (Li, V, 2V, LiV) and supercell sizes (64 and 128 atoms)

Functional	Supercell	E_f (V)	E_f (Li_C)	E_f (2V)	E_f (Li_CV)	2V E_b (V + V)	Li_CV E_b (Li_C + V)
B3LYP	64	6.80 [6.73][77]	8.47 [8.6][44]	9.89 [9.94][82]	9.20	3.72	6.07
	128	6.80	8.54 [8.4][44]	9.90	9.22	3.71	6.12
HSE06	64	7.07 [6.99][77]	8.96 [9.1][44]	10.35 [10.44][82]	9.66	3.80	6.37
PBE0	64	7.13 [7.10][77]	9.02	10.45 [10.53][82]	9.92	3.80	6.23

Comparison of calculated E_f values with referenced values in parentheses; data derived using different functionals.

disorder can complicate the analysis. Fortunately, simulated spectra have become a valuable tool, enabling accurate characterization of spectral features while largely circumventing these complications. The Raman scattering spectra of Li_CV configurations, calculated from equilibrium lattice structures, are presented in Fig. 5, alongside simulated spectra of undefective diamond in the top panel. In these simulations, we utilize the global hybrid functional B3LYP, incorporating 20% non-local exact Hartree–Fock exchange. This functional is favored for its superior performance in capturing the vibrational properties of solids and accurately describing spin states, as indicated by references.[65,86–88] The spectra are plotted using a pseudo-Voigt function, which blends Lorentzian and Gaussian functions, characterized by a full width at half-maximum of 8 cm^{-1}. The precision of the chosen functional and the fine-tuned simulation parameters are demonstrated by the close match between the experimentally measured first-order Raman scattering of triply degenerated phonons of T_{2g} symmetry at 1332 cm^{-1}[88] and the computed value at 1331.6 cm^{-1}, marked by a vertical dashed red line in Fig. 5. Thus, any additional features in the Li_CV spectra are definitively linked to the existing defects.

The introduction of the Li_CV defect disrupts the translational symmetry of pure diamond and diminishes the point symmetry of the crystal, leading to the emergence of new Raman-active modes. These modes manifest with

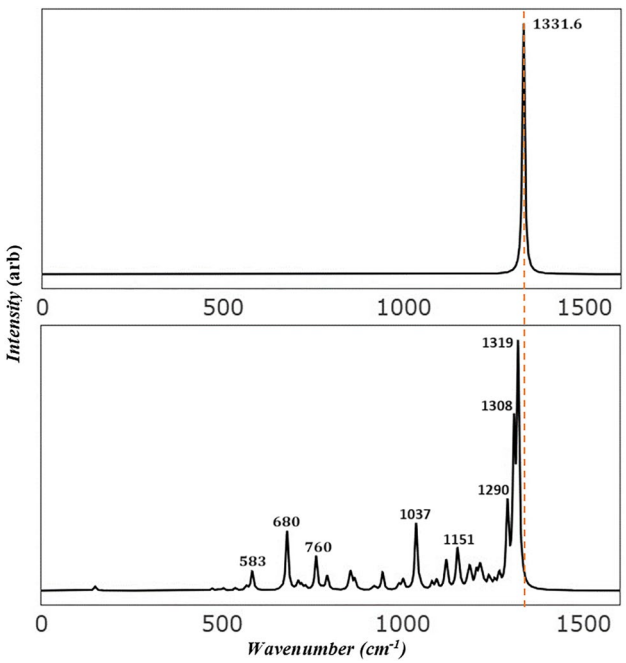

Figure 5 Comparative Raman spectra of diamond and Li_CV defects: *upper panel* the Raman spectra of perfect diamond; *lower panel* the spectra of a diamond with an Li_CV defect. The characteristic diamond peak at 1331.6 cm^{-1} is highlighted with a *red dashed line* across both panels for reference (Color figure online).

significantly lower intensities compared to the primary peak. Analogous to the spectra associated with neutral vacancy defects,[89] no peaks above 1332 cm^{-1} are observed in the Li_CV spectra. A notable characteristic of the Li_CV spectra, in contrast to isolated Li spectra,[65] is the preservation of the primary peak at 1319 cm^{-1}, which is absent in the Li defect. This peak undergoes a red shift of 13 cm^{-1}, mirroring the behavior seen in isolated vacancy spectra.[89] Additionally, the peak exhibits broadening due to a split to 1308 cm^{-1} and is accompanied by a shoulder at 1290 cm^{-1}. The intensities of the newly activated peaks around 1151 cm^{-1} are less pronounced than those observed in isolated vacancy spectra. The current spectra do not display any significant features around or below 400 cm^{-1} , as identified by isolated Li defects.[65] The distinct, non-splitting peaks at 1151, 1037, 760, and 680 cm^{-1} with moderate intensities provide clear indicators to differentiate the vibrational modes associated with isolated Li_CV from those related to isolated Li or V defects.

Conclusions

This study presents the geometry, energy, magnetic properties, and electronic properties of Li_CV defects in diamond. Li_CV can be described as a Li interstitial in the cavity of a two-vacancy within a diamond. The defect is stabilized in three different spin states: ($S_z = ½$) doublet, ($S_z = 3/2$) quartet, and ($S_z = 5/2$) sextet, with relative energies of 0.09 eV and 0.88 eV (B3LYP) compared to the ground ($S_z = 3/2$) quartet state, respectively. The Li atom moves to the midpoint between two vacancies, forming six equivalent bonds with the first neighboring carbon atoms (2.02 Å). The electronic structures of Li_CV defects and 2 V in diamond are discussed in detail. Once formed in diamond, the Li_CV defect is stable due to its high dissociation energy into its constituents, Li_C and V. The binding energy of Li_CV is nearly double that of 2 V, indicating the critical role Li_C plays in controlling and directing V diffusion. The excess charge provided by the Li atom saturates the unpaired electron of the dangling bonds near the 2 V vicinity, resulting in an increased binding energy. In practice, the benefits of the low activation energy of Li_I diffusion can only be exploited by performing diffusion experiments on high-quality, defect-free single crystals, which have recently become available due to significant advances in diamond production. Otherwise, Li_I occupies the vacancy site, forming a Li_C defect which subsequently acts as an active center to trap any residual mobile vacancies, thereby forming a Li_CV defect.

The formation of the Li_CV defect can be effectively detected using Raman spectroscopy, as evidenced by our calculations. These demonstrate a notable red shift of 13 cm^{-1} in the first-order peak, alongside the emergence of newly activated peaks within the range of 500–1319 cm^{-1}.

Crucially, no peaks are observed above the characteristic 1332 cm^{-1} diamond peak, ensuring that the detected features are attributable specifically to the Li_CV defect. This distinct spectral signature provides a reliable means for the experimental identification and study of this defect.

In conclusion, our exploration of Li_CV defects in diamond has unveiled critical insights into the challenges they present for diamond-based semiconductor performance. By addressing these limitations and developing strategies to mitigate their impact, we have taken significant strides towards harnessing the remarkable properties of diamond for advanced electronic applications. This research not only contributes to the field of defect engineering but also paves the way for more efficient, durable, and environmentally friendly devices that can meet the demands of emerging technology sectors.

Author contributions Dr. Tahani Saad Almutairi: Designed the study, collected and analyzed the data, and drafted the manuscript.

Funding The study was supported by the Deanship of Scientific Research at Taibah University.

Conflict of interest The authors declare that they have no affiliations with or involvement in any organization or entity with any financial interest in the subject matter or materials discussed in this manuscript.

Ethical standard All procedures performed in this study were in accordance with the ethical standards of the institutional and/or national research committee and with the 1964 Helsinki Declaration and its later amendments or comparable ethical standards.

Data Access Statement Research data supporting this publication are available upon request from the authors.

References

1. J.E. Field, *The Properties of Natural and Synthetic Diamond* (London: Academic Press, 1992).
2. Neves, A.; Nazar, M. *Properties, Growth and Applications of Diamond*; IET, 2001.
3. M.S. Dresselhaus, and R. Kalish, *Ion Implantation in Diamond, Graphite and Related Materials* (New York: Springer, 2013).
4. L.S. Pan, and D.R. Kania, *Diamond: Electronic Properties and Applications* (New York: Springer, 2013).
5. E. Ekimov, V. Sidorov, E. Bauer, N. Mel'Nik, N. Curro, J. Thompson, and S. Stishov, Superconductivity in diamond. *Nature* 428, 542 (2004). https://doi.org/10.1016/j.diamond.2009.12.002.
6. S. Koizumi, Growth and characterization of phosphorus doped N-type diamond thin films. *Phys. Status Solidi A Appl. Res.* 172(1), 71 (1999). https://doi.org/10.1002/(SICI)1521-396X(199903)172:1%3c71::AID-PSSA71%3e3.0.CO;2-N.
7. L.G. Wang, and A. Zunger, Phosphorus and sulphur doping of diamond. *Phys. Rev. B Condens. Matter Mater. Phys.* 66(16), 1 (2002). https://doi.org/10.1103/PhysRevB.66.161202.
8. R.J. Eyre, J.P. Goss, P.R. Briddon, and J.P. Hagon, Theory of Jahn–Teller distortions of the P donor in diamond. *J. Phys. Condens. Matter* 17(37), 5831 (2005).
9. Y. He, H. Chen, S.J. Poon, and G. Shiflet, The effect of temperature on stability of the Al-Cu-Co decagonal phase. *Philos. Mag. Lett.* 64(5), 307 (1991). https://doi.org/10.1080/09500839108214627.
10. B. Butorac, and A. Mainwood, Symmetry of the phosphorus donor in diamond from first principles. *Phys. Rev. B Condens. Matter Mater. Phys.* 78(23), 1 (2008). https://doi.org/10.1103/PhysRevB.78.235204.
11. S. Koizumi, T. Teraji, and H. Kanda, Phosphorus-doped chemical vapor deposition of diamond. *Diam. Relat. Mater.* 9(3), 935 (2000). https://doi.org/10.1016/S0925-9635(00)00217-X.
12. A.B. Anderson, and L.N. Kostadinov, P and N compensation in diamond molecular orbital theory. *J. Appl. Phys.* 81(1), 264 (1997). https://doi.org/10.1063/1.363993.
13. R. Jones, J.E. Lowther, and J. Goss, Limitations to N-type doping in diamond: the phosphorus-vacancy complex. *Appl. Phys. Lett.* 69(17), 2489 (1996). https://doi.org/10.1063/1.117715.
14. J.P. Goss, P.R. Briddon, R. Jones, and S. Sque, Donor and acceptor states in diamond. *Diam. Relat. Mater.* 13(4–8), 684 (2004). https://doi.org/10.1016/j.diamond.2003.08.028.
15. T. Nishimatsu, H. Katayama-Yoshida, and N. Orita, Theoretical study of hydrogen-related complexes in diamond for low-resistive n-type diamond semiconductor. *Phys. B Condens. Matter* 302–303, 149 (2001). https://doi.org/10.1016/S0921-4526(01)00420-3.
16. T. Miyazaki, and S. Yamasaki, Ab initio energetics of phosphorus related complex defects in synthetic diamond. *Phys. B Condens. Matter* 376–377(1), 304 (2006). https://doi.org/10.1016/j.physb.2005.12.078.
17. A.M. Flatae, S. Lagomarsino, F. Sledz, N. Soltani, S.S. Nicley, K. Haenen, R. Rechenberg, M.F. Becker, S. Sciortino, N. Gelli, L. Giuntini, F. Taccetti, and M. Agio, Silicon-vacancy color centers in phosphorus-doped diamond. *Diam. Relat. Mater.* 105, 107797 (2020). https://doi.org/10.1016/j.diamond.2020.107797.
18. E.B. Lombardi, A. Mainwood, and K. Osuch, Ab initio study of the passivation and interaction of substitutional impurities with hydrogen in diamond. *Diam. Relat. Mater.* 12(3–7), 490 (2003). https://doi.org/10.1016/S0925-9635(02)00233-9.
19. V. Mortet, M. Daenen, T. Teraji, A. Lazea, V. Vorlicek, J. D'Haen, K. Haenen, and M. D'Olieslaeger, Characterization of boron doped diamond epilayers grown in a NIRIM type reactor. *Diam. Relat. Mater.* 17(7–10), 1330 (2008). https://doi.org/10.1016/j.diamond.2008.01.087.
20. K. Nishimura, K. Das, and J.T. Glass, Material and electrical characterization of polycrystalline boron-doped diamond films grown by microwave plasma chemical vapor deposition. *J. Appl. Phys.* 69(5), 3142 (1991). https://doi.org/10.1063/1.348582.
21. J.P. Lagrange, A. Deneuville, and E. Gheeraert, Activation energy in low compensated homoepitaxial boron-doped diamond films. *Diam. Relat. Mater.* 7(9), 1390 (1998). https://doi.org/10.1016/S0925-9635(98)00225-8.
22. E.P. Visser, G.J. Bauhuis, G. Janssen, W. Vollenberg, J.P. Van Enckevort, and L.J. Giling, Electrical conduction in homoepitaxial, boron-doped diamond films. *J. Phys. Condens. Matter* 4(36), 7365 (1992). https://doi.org/10.1088/0953-8984/4/36/011.
23. D.M. Malta, J.A. Von Windheim, H.A. Wynands, and B.A. Fox, Comparison of the electrical properties of simultaneously deposited homoepitaxial and polycrystalline diamond films. *J. Appl. Phys.* 77(4), 1536 (1995). https://doi.org/10.1063/1.358905.
24. J.P. Lagrange, A. Deneuville, and E. Gheeraert, Large range of boron doping with low compensation ratio for homoepitaxial diamond films. *Carbon N. Y.* 37(5), 807 (1999). https://doi.org/10.1016/S0008-6223(98)00275-9.
25. S.A. Kajihara, A. Antonelli, J. Bernholc, and R. Car, Nitrogen and potential N-type dopants in diamond. *Phys. Rev. Lett.* 66(15), 2010 (1991). https://doi.org/10.1103/PhysRevLett.66.2010.

26. E.B. Lombardi, and A. Mainwood, A first principles study of lithium, sodium and aluminum in diamond. *Diam. Relat. Mater.* 17(7–10), 1349 (2008). https://doi.org/10.1016/j.diamond.2007.12.015.
27. J.E. Moussa, N. Marom, N. Sai, and J.R. Chelikowsky, Theoretical design of a shallow donor in diamond by lithium-nitrogen codoping. *Phys. Rev. Lett.* 108(22), 1 (2012). https://doi.org/10.1103/PhysRevLett.108.226404.
28. J. Bernholc, S.A. Kajihara, C. Wang, A. Antonelli, and R.F. Davis, Theory of native defects, doping and diffusion in diamond and silicon carbide. *Mater. Sci. Eng. B* 11(1–4), 265 (1992). https://doi.org/10.1016/0921-5107(92)90222-U.
29. H. Yilmaz, B.R. Weiner, and G. Morell, Formation of lithium clusters and their effects on conductivity in diamond: a density functional theory study. *Diam. Relat. Mater.* 16(4–7 SPEC. ISS.), 840 (2007).
30. A.B. Anderson, and S.P. Mehandru, N-type dopants and conduction-band electrons in diamond: cluster molecular-orbital theory. *Phys. Rev. B* 48(7), 4423 (1993). https://doi.org/10.1103/PhysRevB.48.4423.
31. E.B. Lombardi, A. Mainwood, and K. Osuch, Ab initio study of lithium and sodium in diamond. *Phys. Rev. B Condens. Matter Mater. Phys.* 76(15), 1 (2007). https://doi.org/10.1103/PhysRevB.76.155203.
32. G. Popovici, T. Sung, S. Khasawinah, M.A. Prelas, and R.G. Wilson, Forced Diffusion of Impurities in Natural Diamond and Polycrystalline Diamond Films. *J. Appl. Phys.* 77(11), 5625–5629 (1995). https://doi.org/10.1063/1.359204.
33. G. Popovici, M.A. Prelas, T. Sung, S. Khasawinah, A.A. Melnikov, V.S. Varichenko, A.M. Zaitsev, A.V. Denisenko, and W.R. Fahrner, Properties of diffused diamond films with N-type conductivity. *Diam. Relat. Mater.* 4(5–6), 877 (1995). https://doi.org/10.1016/0925-9635(94)05232-8.
34. C. Cytermann, R. Brener, and R. Kalish, Search for diffusion of Li implants in natural and polycrystalline CVD diamond. *Diam. Relat. Mater.* 3(4–6), 677 (1994). https://doi.org/10.1016/0925-9635(94)90247-X.
35. M.Z. Othman, P.W. May, N.A. Fox, and P.J. Heard, Incorporation of lithium and nitrogen into CVD diamond thin films. *Diam. Relat. Mater.* 44, 1 (2014). https://doi.org/10.1016/j.diamond.2014.02.001.
36. G. Popovici, R.G. Wilson, T. Sung, M.A. Prelas, and S. Khasawinah, Diffusion of boron, lithium, oxygen, hydrogen, and nitrogen in type IIa natural diamond. *J. Appl. Phys.* 77(10), 5103 (1995). https://doi.org/10.1063/1.359320.
37. C. Uzan-Saguy, C. Cytermann, B. Fizgeer, V. Richter, R. Brener, and R. Kalish, Diffusion of lithium in diamond. *Phys. Status Solidi A Appl. Res.* 193(3), 508–516 (2002). https://doi.org/10.1002/1521-396X(200210)193:3%3c508::AID-PSSA508%3e3.0.CO;2-H.
38. K. Okumura, J. Mort, and M. Machonkin, Lithium doping and photoemission of diamond thin films. *Appl. Phys. Lett.* 57(18), 1907 (1990). https://doi.org/10.1063/1.104008.
39. S.C. Halliwell, P.W. May, N.A. Fox, and M.Z. Othman, Investigations of the co-doping of boron and lithium into CVD diamond thin films. *Diam. Relat. Mater.* 76, 115 (2017). https://doi.org/10.1016/j.diamond.2017.05.001.
40. J. te Nijenhuis, G.Z. Cao, P.C.H.J. Smits, W.J.P. van Enckevort, L.J. Giling, P.F.A. Alkemade, M. Nesladek, and Z. Remeš, Incorporation of lithium in single crystal diamond: diffusion profiles and optical and electrical properties. *Diam. Relat. Mater.* 6(11), 1726 (1997).
41. M. Shaanan, and R. Kalish, Simulation of SIMS measurements of light element profiles in diamond. *Nucl. Instrum. Methods Phys. Res. B* 171(3), 332 (2000). https://doi.org/10.1016/S0168-583X(00)00265-2.
42. E.B. Lombardi, and A. Mainwood, Li and Na in diamond: a comparison of DFT models. *Phys. B Condens. Matter* 401–402, 57 (2007). https://doi.org/10.1016/j.physb.2007.08.113.
43. J.P. Goss, and P.R. Briddon, Theoretical study of Li and Na as n -type dopants for diamond. *Phys. Rev. B Condens. Matter Mater. Phys.* 75(7), 1–9 (2007). https://doi.org/10.1103/PhysRevB.75.075202.
44. S. Conejeros, M.Z. Othman, A. Croot, J.N. Hart, K.M. O'Donnell, P.W. May, and N.L. Allan, Hunting the elusive shallow N-type donor—an ab initio study of Li and N co-doped diamond. *Carbon N. Y.* 171, 857 (2021). https://doi.org/10.1016/j.carbon.2020.09.065.
45. P. Hohenberg, and W. Kohn, Inhomogeneous electron gas. *Phys. Rev.* 136, B864 (1964).
46. W. Kohn, and L.J. Sham, *Phys. Rev.* 140, A1133 (1965).
47. Becke, A. D. Density-functional Thermochemistry. I. The Effect of the Exchange-only Gradient Correction. *J. Chem. Phys* **1992**, *3* (96), 2155–2160. https://doi.org/10.1063/1.462066.
48. R. Dovesi, R. Orlando, A. Erba, C.M. Zicovich-Wilson, B. Civalleri, S. Casassa, L. Maschio, M. Ferrabone, M.D. La Pierre, P.D. Arco, Y. No, and M. Caus, C RYSTAL 14: a program for the ab initio investigation of crystalline solids. *Int. J. Quantum Chem.* 114(19), 1287 (2014). https://doi.org/10.1002/qua.24658.
49. C. Adamo, and V. Barone, Toward chemical accuracy in the computation of NMR shieldings: the PBE0 model. *Chem. Phys. Lett.* 298(1–3), 113 (1998). https://doi.org/10.1016/S0009-2614(98)01201-9.
50. A.V. Krukau, O.A. Vydrov, A.F. Izmaylov, and G.E. Scuseria, Influence of the exchange screening parameter on the performance of screened hybrid functionals. *J. Chem. Phys.* (2006). https://doi.org/10.1063/1.2404663.
51. M. Catti, A. Pavese, R. Dovesi, and V.R. Saunders, Static lattice and electron properties of $MgCO_3$ (magnesite) calculated by ab initio periodic Hartree–Fock method. *Phys. Rev. B* 47(15), 9189 (1993).
52. R. Dovesi, M. Causa', R. Orlando, C. Roetti, and V.R. Saunders, Ab initio approach to molecular crystals: a periodic Hartree–Fock study of crystalline urea. *J. Chem. Phys.* 92(12), 7402 (1990). https://doi.org/10.1063/1.458592.
53. M.F. Peintinger, D.V. Oliveira, and T. Bredow, Consistent Gaussian basis sets of triple-zeta valence with polarization quality for solid-state calculations. *J. Comput. Chem.* 813, 451 (2013). https://doi.org/10.1002/jcc.23153.
54. H.J. Monkhorst, and J.D. Pack, Special points for Brillouin-zone integrations. *Phys. Rev. B* 13(12), 5188 (1976). https://doi.org/10.1103/PhysRevB.13.5188.
55. C. Pisani, R. Dovesi, and C. Roetti, *Hartree–Fock ab initio treatment of crystalline systems. Lecture Notes in Chemistry* (Berlin: Springer, 2012).
56. R.S. Mulliken, Electronic population analysis on LCAO-MO molecular wave functions. I. *J. Chem. Phys.* 23(10), 1833 (1955).
57. www.ioffe.ru/SVA/NSM/Semicond/Diamond/basic.html.
58. A.M. Ferrari, S. Salustro, F.S. Gentile, W.C. Mackrodt, and R. Dovesi, Substitutional nitrogen atom in Diamond. A quantum mechanical investigation of the electronic and spectroscopic properties. *Carbon N Y* 134, 354 (2018).
59. A.M. Zaitsev, *Optical Properties of Diamond A Data Handbook* (New York: Springer, 2013).
60. Walkert, J. *Optical Absorption and Luminescence in Diamond*; 1979; Vol. 42.
61. C.M. Zicovich-Wilson, F. Pascale, C. Roetti, V.R. Saunders, R. Orlando, and R. Dovesi, Calculation of the vibration frequencies of α-quartz: the effect of Hamiltonian and basis set. *J. Comput. Chem.* 25(15), 1873 (2004).
62. F. Pascale, C.M. Zicovich-Wilson, F. Lopez, B. Civalleri, R. Orlando, and R. D., The calculation of the vibrational frequencies

of crystalline compounds and its implementation in the CRYSTAL code. *J. Comput. Chem.* 25, 888 (2004).
63. L. Maschio, B. Kirtman, M. Rérat, R. Orlando, and R. Dovesi, Ab initio analytical Raman intensities for periodic systems through a coupled perturbed Hartree–Fock/Kohn–Sham method in an atomic orbital basis. I. Theory. *J. Chem. Phys.* 139(16), 164101 (2013).
64. L. Maschio, B. Kirtman, R. Orlando, and M. Rèrat, Ab initio analytical infrared intensities for periodic systems through a coupled perturbed Hartree–Fock/Kohn–Sham method. *J. Chem. Phys.* 137(20), 204113 (2012).
65. F.S. Gentile, W.C. Mackrodt, N.L. Allan, and R. Dovesi, Predicted strong spin-phonon interactions in Li-doped diamond. *Phys. Chem. Chem. Phys.* 22(36), 20612–20617 (2020).
66. P. Deák, B. Aradi, M. Kaviani, T. Frauenheim, and A. Gali, Formation of NV centers in diamond: a theoretical study based on calculated transitions and migration of nitrogen and vacancy related defects. *Phys. Rev. B Condens. Matter Mater. Phys.* 89(7), 1 (2014).
67. A. Mainwood, Nitrogen and nitrogen-vacancy complexes and their formation in diamond. *Phys. Rev. B* 49(12), 7934 (1994). https://doi.org/10.1103/PhysRevB.49.7934.
68. E. Rohrer, C.F.O. Graeff, R. Janssen, C.E. Nebel, and M. Stutzmann, Nitrogen-related dopant and defect states in CVD diamond. *Phys. Rev. B* 54, 90 (1996). https://doi.org/10.1103/PhysRevB.54.7874.
69. R.G. Farrer, On the substitutional nitrogen donor in diamond. *Solid State Commun.* 7(9), 685 (1969). https://doi.org/10.1016/0038-1098(69)90593-6.
70. E.B. Lombardi, K. Alison-Mainwood, and A. Osuch, Interaction of hydrogen with boron, phosphorus, and sulfur in diamond. *Phys. Rev. B* 70(20), 205201 (2004).
71. S. Salustro, F. Colasuonno, A.M. Ferrari, M. d'Amore, W.C. Mackrodt, and R. Dovesi, Substitutional boron and nitrogen pairs in diamond A quantum mechanical vibrational analysis. *Carbon N Y* 146, 709 (2019). https://doi.org/10.1016/j.carbon.2019.01.072.
72. F.S. Gentile, S. Salustro, G. Di Palma, M. Causà, P. D'Arco, and R. Dovesi, Hydrogen, boron and nitrogen atoms in diamond: a quantum mechanical vibrational analysis. *Theor. Chem. Acc.* 137(11), 1 (2018). https://doi.org/10.1007/s00214-018-2375-0.
73. S.J. Breuer, and P.R. Briddon, Ab initio investigation of the native defects in diamond and self-diffusion. *Phys. Rev. B* 51(11), 6984 (1995). https://doi.org/10.1103/PhysRevB.51.6984.
74. J. Walker, Optical absorption and luminescence in diamond. *Rep. Prog. Phys.* 42(10), 1605 (1979). https://doi.org/10.1088/0034-4885/42/10/001.
75. H.A. Jahn, and E. Teller, Stability of polyatomic molecules in degenerate electronic states I—orbital degeneracy. *Proc. R. Soc.* 61(905), 220 (1937).
76. T.S. Almutairi, Theoretical and Experimental Investigation of N-Type Doped Diamond . Doctoral dissertation, University of Bristol, Bristol, 2021. https://research-information.bris.ac.uk/ws/portalfiles/portal/271158416/THEORETICAL_AND_EXPERIMENTAL_INVESTIGATION_OF_N_TYPE_DOPED_DIAMOND.pdf. Accessed 07 Aug 2022.
77. A. Zelferino, S. Salustro, J. Baima, V. Lacivita, R. Orlando, and R. Dovesi, The electronic states of the neutral vacancy in diamond: a quantum mechanical approach. *Theor. Chem. Acc.* 135(3), 1 (2016). https://doi.org/10.1007/s00214-016-1813-0.
78. G. Sansone, S. Salustro, Y. Noël, L. Maschio, W.C. Mackrodt, and R. Dovesi, Looking for Sp2 carbon atoms in diamond: a quantum mechanical study of interacting vacancies. *Theor. Chem. Acc.* 137(2), 1 (2018). https://doi.org/10.1007/s00214-018-2201-8.
79. G. Davies, S.C. Lawson, T. Collins, A. Mainwood, and J. Sharp, Vacancy-related centers in diamond. *Phys. Rev.* 46(20), 13157 (1992).
80. L. Webster, L. Liang, and J.-A. Yan, Distinct spin-lattice and spin-phonon interactions in monolayer magnetic CrI3. *Phys. Chem. Chem. Phys.* 20(36), 23546 (2018).
81. A. Croot, M.Z. Othman, S. Conejeros, N.A. Fox, and N.L. Allan, A theoretical study of substitutional boron-nitrogen clusters in diamond. *J. Phys. Condens. Matter* 30(42), 425501 (2018). https://doi.org/10.1088/1361-648X/aade16.
82. G. Sansone, S. Salustro, Y. Noël, L. Maschio, W.C. Mackrodt, and R. Dovesi, Looking for Sp2 carbon atoms in diamond: a quantum mechanical study of interacting vacancies. *Theor. Chem. Acc.* (2018). https://doi.org/10.1007/s00214-018-2201-8.
83. A.T. Collins, Vacancy enhanced aggregation of nitrogen in diamond. *J. Phys. C Solid State Phys.* 13(14), 2641–2650 (1980). https://doi.org/10.1088/0022-3719/13/14/006.
84. R. Jones, and J.P. Goss, Theory of aggregation of nitrogen in diamond. *EMIS Datarev. Ser.* 26, 127 (2002).
85. T. Evans, and Z. Qi, The kinetics of the aggregation of nitrogen atoms in diamond. *Proc. R. Soc. A Math. Phys. Eng. Sci.* 381(1780), 159 (2006). https://doi.org/10.1098/rspa.1982.0063.
86. R. Dovesi, R. Orlando, A. Erba, C.M. Zicovich-Wilson, B. Civalleri, S. Casassa, L. Maschio, M. Ferrabone, M. De La Pierre, P. d'Arco, and Y. Noël, CRYSTAL14: a program for the ab initio investigation of crystalline solids. *Int. J. Quant. Chem.* 15, 1287 (2014).
87. M. De La Pierre, R. Orlando, L. Maschio, K. Doll, P. Ugliengo, and R. Dovesi, Performance of six functionals (LDA, PBE, PBESOL, B3LYP, PBE0, and WC1LYP) in the simulation of vibrational and dielectric properties of crystalline compounds. The case of forsterite Mg_2SiO_4. *J. Comput. Chem.* 32(9), 1775 (2011).
88. S. Solin, and A. Ramdas, Raman spectrum of diamond. *Phys. Rev. B* 1(4), 1687 (1970).
89. J. Baima, A. Zelferino, P. Olivero, A. Erba, and R. Dovesi, Raman spectroscopic features of the neutral vacancy in diamond from ab initio quantum-mechanical calculations. *Phys. Chem. Chem. Phys.* 18(3), 1961 (2016).